

1 **Improved GRACE regional mass balance estimates of the**
2 **Greenland Ice Sheet cross-validated with the input-output method**

3 **Z.Xu¹, E.Schrama¹, W. van der Wal¹, M. van den Broeke², Ellyn M. Enderlin³**

4 [1] Faculty of Aerospace Engineering, Delft University of Technology, the Netherlands.

5 [2] Institute for Marine and Atmospheric Research, Utrecht University (UU/IMAU), the
6 Netherlands

7 [3] Climate Change Institute & School of Earth and Climate Science, University of Maine, Orono,
8 ME 04469, USA

9 Correspondence to: Z.Xu (Z.Xu-1@tudelft.nl)

1 **Abstract**

2 In this study, we use satellite gravimetry data from the Gravity Recovery and Climate Experiment
3 (GRACE) to estimate regional mass changes of the Greenland ice sheet (GrIS) and neighbouring
4 glaciated regions using a least-squares inversion approach. We also consider results from the input-
5 output method (IOM) that quantifies the difference between mass input and output of the surface
6 mass balance (SMB) components from the Regional Atmospheric Climate Model version 2
7 (RACMO2) and ice discharge (D) from 12 years of high-precision ice velocity and thickness
8 surveys.

9 We use a simulation model to quantify and correct for GRACE approximation errors in mass
10 changes between different sub-regions of GrIS and investigate the reliability of pre-1990s ice
11 discharge estimates based on modelled runoff. We find that the difference between IOM and our
12 improved GRACE mass change estimates is reduced in terms of the long-term mass changes, when
13 using a reference discharge derived from the runoff estimates in several sub-areas. In most regions
14 our GRACE and IOM solutions are consistent with other studies, but differences remain in the
15 northwestern GrIS. We verify the GRACE mass balance in that region by considering several
16 different GIA models and mass change estimates derived from the Ice, Cloud and land Elevation
17 satellite (ICESat). We conclude that the remaining differences between GRACE and IOM are likely
18 due to underestimated uncertainties in the IOM solutions.

19

1 **1 Introduction**

2 During the last decade, the ice mass loss from the Greenland ice sheet (GrIS) became one of the
3 most significant mass changing events on Earth. Because of its ongoing and potentially large future
4 contribution to sea level rise, it is critical to understand the mass balance of the GrIS in detail. As
5 the result of increasing run-off and solid ice discharge, the GrIS has been experiencing a
6 considerable and increasing mass loss since the mid-1990s (Hanna et al., 2005; Rignot and
7 Kanagaratnam, 2006; van den Broeke et al., 2009). The changes in mass loss rates are due to
8 different processes, e.g. in the northwestern GrIS the mass loss acceleration is linked to the rapidly
9 increasing discharge in this region (Enderlin et al., 2014; Andersen et al., 2015), while in the
10 southeast the increase in mass loss rate after 2003 is mainly due to enhanced melting and less
11 snowfall (Noël et al., 2015).

12 To quantify recent changes in GrIS mass balance, three methods are used: satellite altimetry,
13 satellite gravimetry and the input-output method (Andersen et al., 2015; Colgan et al., 2013; Sasgen
14 et al., 2012; Shepherd et al., 2012; Velicogna et al., 2014; Wouters et al., 2013). The latter two
15 methods are used for this study.

16 The input/output method (IOM) evaluates the difference between mass input and output for a
17 certain region. It considers two major mass change entities, i.e. Surface mass balance (SMB) and
18 solid ice discharge (D). SMB is commonly estimated using climate models (Ettema et al., 2009;
19 Fettweis, 2007; Tedesco et al., 2013; van Angelen et al., 2012), whereas ice discharge can be
20 estimated with combined measurements of ice velocity and the ice thickness, e.g. Rignot and
21 Kanagaratnam (2006), Enderlin et al. (2014) and Andersen et al. (2015). The total SMB and D
22 from 1960 to 1990 are sometimes used in order to reduce the uncertainties in the mass changes of

1 SMB and D (van den Broeke et al., 2009; Sasgen et al., 2012). However, using the reference SMB
2 and D may introduce new uncertainties in IOM. We will discuss the details of the IOM as well as
3 the uncertainties of the reference SMB and D in Sect. 2.

4 The satellite gravity observations from GRACE (Gravity Recovery and Climate Experiment),
5 provide snapshots of the global gravity field at monthly time intervals. which can be converted to
6 mass variations. GRACE observations are, however, influenced by measurement noise and leakage
7 of signals caused by mass changes in neighboring areas. Besides, the GRACE data contain north-
8 south oriented stripes due to measurement noise and mis-modeled high-frequency signal aliasing
9 in the monthly gravity fields. Therefore, in order to estimate the mass balance for GrIS sub-regions
10 from GRACE data, we apply the Least Squares inversion method (Schrama and Wouters, 2011) in
11 this study with an improved approach to obtain constraints (Xu et al., 2015). Bonin and Chambers
12 (2013) showed in a simulation study that the Least Squares inversion method introduces errors. In
13 this study, we aim to tackle the error from the inversion approach as well as the effect of different
14 discharge estimates resulting from assumptions about discharge during a reference period. We then
15 evaluate our results by comparing GRACE and IOM estimates with each other and with published
16 estimates from satellite altimetry. Previous studies have compared regional GrIS mass changes
17 from different independent methods. In Sasgen et al. (2012), the mass balance in 7 major GrIS
18 basins was derived from the IOM and GRACE data using a forward modelling approach (Sasgen
19 et al., 2010). When separating out the IOM components and comparing with the seasonal variability
20 in the derived GRACE solution the relative contributions of SMB and D to the annual mass
21 balances were revealed. In the northwestern GrIS important differences between IOM and GRACE
22 were noted, which were ascribed to the uncertainty in the regional discharge component in this area
23 where detailed surveys of ice thickness are lacking. The comparison between two approaches

1 shows $24 \pm 13 \text{ Gt}\cdot\text{yr}^{-1}$ mass loss difference in this region, and as a result the uncertainty in the
2 regional mass balance estimate is estimated at $\sim 46\%$. However, using new discharge estimates and
3 the corresponding IOM regional mass changes in the northwestern GrIS, Andersen et al. (2015)
4 found that the difference between GRACE and IOM mass loss estimates fell within the combined
5 uncertainty range

6 The GrIS drainage systems (DS) definition of Zwally (2012) is employed in order to investigate
7 the mass balance in GrIS sub-region. This definition divides the whole GrIS into 8 major drainage
8 areas, and each drainage area is further separated by the 2000m elevation contour line, creating the
9 interior and coastal regions for each drainage area. This GrIS DS definition is employed by several
10 other studies, (Andersen et al., 2015; Barletta et al., 2013; Colgan et al., 2013; Luthcke et al., 2013;
11 Sasgen et al., 2012). Also, Wouters et al. (2008) found that in GRACE data, the regional mass
12 changes on GrIS are also influenced by the mass changes in areas outside Greenland, i.e. Ellesmere
13 Island, Baffin Island, Iceland and Svalbard (EBIS) (Wouters et al. 2008). Therefore, we include
14 four additional DS to reduce the leakage from these regions; the overall mascon definition used in
15 this study are shown in Fig. 1.

16 Using the Least Squares based inversion approach of Schrama and Wouters (2011), we find that
17 mass change differences between GRACE and IOM in the southern GrIS are larger than the
18 assumed uncertainties. An example of the regional difference between the GRACE data and the
19 IOM solution can be seen in Fig. A1. The details of this difference will be discussed in Sect. 4.

20 The main topic of this study is to provide improved GrIS regional mass balance estimates from
21 GRACE and the IOM. We show that the improved GRACE solution brings down the regional
22 differences between two mass changes estimates, mainly in the southeast GrIS region. Furthermore,

1 we compare the GRACE solution with the IOM, which employs different reference discharge
2 estimates, showing that the uncertainties in the reference discharge can result in underestimated
3 mass loss rate in the IOM regional solution in particular in the northwest GrIS region.

4 In Sect. 2, we present SMB mass changes from a recently improved regional atmospheric climate
5 model (RACMO2) (Noël et al., 2015) and discharge estimates of Enderlin et al. (2014), which are
6 based on a near-complete survey of the ice thickness and velocity of Greenland marine-terminating
7 glaciers. In Sect. 3, we introduce the Least Squares inversion approach. In Sect. 4, we firstly
8 investigate different methods to calculate mass changes in basins using the modelled SMB and D
9 estimates. Then we identify the approximation errors in regional mass change estimates from
10 GRACE data. In the end we compare mass change estimates from GRACE and IOM, and discuss
11 remaining differences. Conclusions and recommendations are given in Sect 5.

12 **2 IOM method**

13 *2.1. SMB and D*

14 For the GrIS, precipitation (P) in the form of snowfall is the main contribution to the mass input,
15 while mass loss is a combination of sublimation (S), melt water runoff (R), and solid ice discharge
16 (D). Surface mass balance (SMB) equals to $P - S - R$, and subtracting D from SMB yields the total
17 mass balance (TMB). In this study, we use the Regional Atmospheric Climate Model, version 3
18 (RACMO2.3) to model the SMB of the GrIS. RACMO2 (Ettema et al., 2009; van Angelen et al.,
19 2012; van den Broeke et al., 2009) is developed and maintained at the Royal Netherlands
20 Meteorological Institute (KNMI) and has been adapted for the polar regions at the Institute for
21 Marine and Atmospheric Research, Utrecht University (UU/IMAU). RACMO2 model output is

1 currently available at $\sim 0.1^\circ$ spatial resolution for Jan 1958 to Dec 2014. The differences between
2 a previous model version (RACMO2.1) and other SMB models are discussed by Vernon et al.
3 (2013). In RACMO2 we assume 20% uncertainties for the P and R components in each grid cell.
4 Assuming both components to be independent, the uncertainty of the SMB is the quadratic sum of
5 uncertainties of P and R. Note that the magnitude of S is small and its absolute uncertainty
6 negligible compared to those in P and R. Note that the RACMO2 model also provides the estimates
7 of SMB in the peripheral glacier areas, which we have included in this study.

8 Ice discharge (D) estimates from Enderlin et al. (2014) (hereafter Enderlin-14, with the associated
9 discharge estimates D-14) are used in this study. In Enderlin-14, the ice thickness of 178 glaciers
10 is estimated as the difference in ice surface elevations from repeat digital elevation models and bed
11 elevations from NASA's Operation IceBridge airborne ice-penetrating radar data while the ice
12 surface velocity is obtained from tracking the movement of surface features visible in repeat
13 Landsat 7 Enhanced Thematic Mapper Plus and Advanced Spaceborne Thermal and Reflectance
14 Radiometer (ASTER) images. For glaciers with thickness transects perpendicular to ice flow (i.e.,
15 flux gates), the ice flux is estimated by summing the product of the ice thickness and surface speed
16 across the glacier width. Ice flux for glaciers with only centreline or without thickness estimates is
17 based on empirical scaling factors as derived in Enderlin et al. (2014). Because the ice fluxes are
18 calculated within 5 km of the estimated grounding line locations, SMB gain or loss between the
19 observations and the grounding lines will be small and the ice discharge is estimated directly from
20 the fluxes (Enderlin et al., 2014). The estimation of discharge uncertainty of 1~5% D for each
21 glacier is smaller than in previous studies, e.g. Rignot et al. (2008) (hereafter Rignot-08, and the
22 associated estimates are denoted by D-08), which relied on interior ice thickness estimates that
23 were assumed constant in time.

1 2.2. *Cumulative TMB anomaly*

2 For the whole GrIS or a complete basin from ice sheet maximum height to the coast, the total mass
3 balance is:

$$4 \quad \text{TMB} = \text{SMB} - \text{D} \quad (1)$$

5 In this study, we further separate each GrIS basin in a downstream (I) and upstream (II) region
6 separated by the 2000m surface elevation contour line. Thus, for the sub-divided regions Eq. (1)
7 becomes:

$$8 \quad \text{TMB} = \text{TMB}^{\text{I}} + \text{TMB}^{\text{II}} \quad (2)$$

9 where

$$10 \quad \text{TMB}^{\text{II}} = \text{SMB}^{\text{II}} - \text{F}^{\text{II}}$$

$$11 \quad (3)$$

12 and

$$13 \quad \text{TMB}^{\text{I}} = \text{SMB}^{\text{I}} + \text{F}^{\text{II}} - \text{F}^{\text{I}}$$

$$14 \quad (4)$$

15 in which F^{II} refers to the ice flux across the 2000 m elevation contour, and F^{I} refers to the ice flow
16 across the flux gate. Note that F^{II} is cancelled if the study area includes both the regions below and
17 above the 2000m contour, but F^{II} has to be considered when the upstream and downstream regions
18 are considered separately. As described above, we assume that SMB changes downstream of the
19 Enderlin-14 flux gates are negligible and that $\text{F}^{\text{I}} = \text{D}$.

1 In order to fit the temporal resolution of the modeled SMB data, we interpolate the yearly D on a
 2 monthly basis. Significant seasonal variations in ice velocity have been observed along
 3 Greenland's marine-terminating outlet glaciers (Moon et al., 2014). However, since we focus
 4 mostly on long-term changes in mass in this study, monthly variations in D should have a negligible
 5 influence on our analysis and we assume that D is approximately constant throughout the year. The
 6 monthly GRACE data represent the gravity field of Earth at that particular month. By subtracting
 7 the gravity field from a reference period (e.g. the 2003 – 2014 average), the gravity variations with
 8 respect to this reference can be obtained. These can be converted to mass variations assuming that
 9 all mass variation takes place in a thin layer near to the Earth's surface. Contrary to the GRACE
 10 data, the SMB, D and TMB are estimates of rates of mass change (i.e., mass flux) in Gt per month.
 11 Hence in order to compare with GRACE, one has to integrate the SMB and D from a certain month
 12 (or year), which yields:

$$13 \quad \Delta TMB_i = \int_{i_0}^i (SMB_t - D_t) dt \quad (5)$$

14 where ΔTMB_i is the cumulative mass change at month i in the IOM (unit is Gt) and the integration
 15 time period is from a certain initial month i_0 to month i .

16 In previous studies of mass balance using the IOM, when estimates of D were not available for
 17 some regions (Rignot et al., 2008), the 1961 to 1990 reference SMB was used to approximate the
 18 missing regional D (Sasgen et al., 2012). Also, due to the uncertainties in the SMB model,
 19 accumulating the TMB over a long time period may lead to unrealistic mass gains or losses (van
 20 den Broeke et al., 2009). By removing the reference, the influence of the large uncertainties and
 21 inter-annual variability in SMB and D can be reduced (van den Broeke et al., 2009). The reference

1 period is chosen based on the assumption that the mass gain from the surface mass balance during
 2 that period is compensated by ice discharge, so the GrIS was in balance (i.e. no mass change).

3 For the reference period we define the month index to run from i_0 to i_1 , and from i_2 to i afterwards.

4 Since we assume the GrIS was in balance during this period, $\int_{i_0}^{i_1} (\text{SMB}_t - D_t) dt = 0$. By removing
 5 the reference SMB and D (i.e. SMB_0 and D_0) Eq. (5) becomes:

$$6 \quad \Delta \text{TMB}_i = \int_{i_2}^i (\delta \text{SMB}_t - \delta D_t) dt \quad (6)$$

7 where $i \geq i_2$, $\delta \text{SMB}_i = \text{SMB}_i - \text{SMB}_0$ and $\delta D_i = D_i - D_0$. Note that SMB_0 and δSMB_i are both
 8 rates of mass change, similar to the discharge.

9 As explained before, when Eq. (6) is used to compute the mass balance for the regions below and
 10 above 2000m separately, the ice flux across the 2000m contour (F^{II}) has to be considered. Because
 11 this flux can not be easily measured we introduce two assumptions, i.e. 1) F^{II} is constant over time,
 12 which means $F^{\text{II}} = F_0^{\text{II}}$ (F_0^{II} is the F^{II} during the reference period), so $\int_{i_2}^i \delta F_t^{\text{II}} dt = 0$, and 2) the
 13 separate GrIS interior and coastal regions are all in balance during the 1961 – 1990 reference period,
 14 i.e. $\int_{i_0}^{i_1} (\text{SMB}_0^{\text{II}} - F_0^{\text{II}}) dt = 0$ and $\int_{i_0}^{i_1} (\text{SMB}_0^{\text{I}} + F_0^{\text{II}} - D_0) dt = 0$ Assumption 1) is necessary since
 15 there is a lack of yearly measurements of ice velocity across the 2000m contour. An estimate of
 16 decadal change by Howat et al. (2011) suggests it is reasonable to assume a constant F^{II} for the
 17 entire GrIS, except for a few glaciers, such as the Jakobshavn glacier in basin 7 where the F^{II} may
 18 be higher than F_0^{II} after 2000. In Andersen et al. (2015), the mass balance of the interior GrIS (in
 19 their study defined as the ice sheet above the 1700 m elevation contour) was $41 \pm 61 \text{ Gt}\cdot\text{yr}^{-1}$ during
 20 the 1961-1990 reference period and in Colgan et al. (2015) the ice flux across the 1700m contour

1 was estimated to be $54 \pm 46 \text{ Gt}\cdot\text{yr}^{-1}$ for the same time period, indicating the assumption of balance
 2 approximately holds within the uncertainties.

3 Based on these two assumptions, we apply Eq. (6) to the interior and coastal GrIS regions, yielding:

$$4 \quad \Delta\text{TMB}_i^{\text{II}} = \int_{i_2}^i \text{SMB}_t^{\text{II}} dt \quad (7)$$

5 And

$$6 \quad \Delta\text{TMB}_i^{\text{I}} = \int_{i_2}^i (\text{SMB}_t^{\text{I}} - D_t) dt \quad (8)$$

7 We quantify the combined uncertainties of assumptions 1) and 2) by comparing the results from
 8 Eq. (8) to the regional mass balance derived from GRACE by Wouters and Schrama (2008) and
 9 derived from ICESat by Zwally et al. (2011), resulting in $\sim \pm 15 \text{ Gt}\cdot\text{yr}^{-1}$ uncertainties for the entire
 10 interior GrIS. The regional uncertainties are summarized in Table A2. Note that for each region,
 11 the same uncertainty is applied to both the interior and coastal areas. For the whole basin the
 12 uncertainties associated with assumption 1) and 2) will vanish, because these two assumptions are
 13 needed only when we separate the coastal and interior regions.

14

15 **3 GRACE**

16 *3.1. Post-processing GRACE data*

17 In this study we use the GRACE release 5 level 2 monthly spherical harmonics coefficients C_{lm}
 18 and S_{lm} ('*GSM*') produced by the University of Texas Center for Space Research (CSR). The time
 19 interval is from Jan 2003 to Jan 2014 and the maximum spherical harmonic degree $l = 60$. We add

1 C_{10} , C_{11} and S_{11} coefficients (related to the motion of the Earth's geocenter) obtained from GRACE
2 data and independent oceanic and atmospheric models (Swenson et al., 2008). The geopotential
3 flattening coefficients (C_{20}) in GRACE data are less accurate than those from Satellite Laser
4 Ranging (SLR) measurements (Chen et al., 2004). We replace these coefficients with the ones from
5 Cheng et al. (2013). The GRACE potential coefficients are averaged between Jan 2003 and Jan
6 2014 and this average field serves as a reference to obtain monthly anomalies ΔC_{lm} and ΔS_{lm} .

7 GRACE observations of mass change within a sub-region of the GrIS are affected by mass changes
8 in neighbouring areas, a phenomenon known as leakage (Wahr et al., 1998). GRACE data should
9 also be corrected for known oceanic and atmospheric mass motions, continental hydrology and
10 Glacial Isostatic Adjustment (GIA). The oceanic and atmospheric mass changes are already
11 removed from the coefficients provided by CSR. The Global Land Data Assimilation System
12 (GLDAS) model (Rodell et al., 2004) is employed to simulate the continental hydrology, which is
13 then removed from the GRACE monthly coefficients. Note that permafrost regions are excluded
14 in the GLDAS version 2 1° monthly data that are obtained from Goddard Earth Sciences Data and
15 Information Services Center.

16 The GIA effect in the GRACE data for the GrIS is compensated via the model output of Paulson
17 et al., (2007), which is based on an the ICE-5G ice loading history and the VM2 Earth model
18 (Peltier 2004). Hereafter we refer to this model by Paulson-07. In addition to this model, 11
19 alternative GIA models are employed based on different ice history and viscosity models to
20 determine the uncertainty in the GIA correction. For instance, the models of van der Wal et al.,
21 (2013) include 3D changes in viscosity and the model of Simpson et al. (2009) uses a different ice
22 loading history, see the summary of the GIA models used in this study in Table A3. An isotropic

1 Gaussian filter is employed to reduce the noise in GRACE data (Wahr et al. 1998), with a half
2 width of $r_{1/2}=300\text{km}$.

3 3.2. *Inversion of the regional mass balance*

4 To estimate the regional mass balance in separate GrIS basins, we apply a constrained least-squares
5 inversion approach (Bonin and Chambers, 2013; Schrama and Wouters, 2011).

$$\hat{\mathbf{x}} = (\mathbf{H}^T \mathbf{H} + \mathbf{P}^{-1})^{-1} \mathbf{H}^T \mathbf{y} \quad (9)$$

6 The vector \mathbf{y} contains the monthly GRACE data. To compute the influence functions in the design
7 matrix \mathbf{H} we assume a layer of water with unit height uniformly distributed over the mascon, then
8 express the mass change in spherical harmonic coefficients up to degree and order (d/o) 60, similar
9 to the GRACE data. The vector $\hat{\mathbf{x}}$ represents the scale factors for the unit mass changes in each
10 basin that we aim to find. \mathbf{P} is the covariance matrix of the mass changes in each mascon. When
11 assuming that the mass changes in each equally weighted mascon are independent then $\mathbf{P} = \lambda \mathbf{I}$,
12 with λ the prior variance of the regional mass changes. In our previous study, we demonstrated that
13 three different prior variances for the GrIS regions below and above 2000m, as well as for the
14 surrounding Arctic regions respectively improved the recovery of regional mass changes (Xu et al.
15 2015). Using a simulation model based on the IOM (see Sect. A3) optimal regional constraints
16 were determined, i.e. for coastal mascons $\lambda_{\mathbf{a}} = 13\text{m}^2$, for inland mascons $\lambda_{\mathbf{b}} = 0.1\text{m}^2$ and for the
17 nearby surrounding EBIS regions (Ellesmere island, Baffin island, Iceland and Svalbard) $\lambda_{\text{EBIS}} =$
18 11m^2 .

1 **4 Cross-validation**

2 *4.1. Reference SMB and D*

3 In this study, the error in SMB_0 , hereafter σSMB_0 involves the systematic error caused by the
 4 assumption of a reference period and the fact that averaging within the chosen reference period
 5 results in an error. Both parts will be explained hereafter.

6 The systematic error is the uncertainty in the SMB derived from model output and the averaging
 7 error is related to the variability of the reference SMB_0 during 1961-1990. To quantify the latter,
 8 we apply a Monte-Carlo simulation to evaluate the standard deviations of the SMB_0 resulting from
 9 using different combinations of a 20-year average of SMB. The sampled combinations are
 10 randomly chosen from the months between 1961 and 1990, following van den Broeke et al. (2009).
 11 For RACMO2, we find 20 $Gt \cdot yr^{-1}$ averaging errors in σSMB_0 . The SMB_0 from RACMO2 yields
 12 403 $Gt \cdot yr^{-1}$ hence the systematic error is approximately 73 $Gt \cdot yr^{-1}$ (considering 18% uncertainty
 13 in RACMO2). If we assume both errors are independent then $\sigma SMB_0 = 75 Gt \cdot yr^{-1}$.

14 We also investigate the uncertainties of the 1961 – 1990 reference discharge. In this study we
 15 employ D-14 as the D estimates in IOM. However the D-14 time series starts from the year of 2000
 16 when the GrIS already was significantly out of balance. In order to retrieve D_0 for D-14 (D_0 -14),
 17 we employ the $D_0 = 413 Gt \cdot yr^{-1}$ in 1996 from D-08 (D_0 -08) for the entire GrIS, and assume that the
 18 regional D changes from 1990 to 2000 in D-08 are proportional to the changes in D-14 in each
 19 region, i.e. D-14 and D-08 are linearly related. The details of the interpolation of the regional D_0
 20 are given in Sect. A1. Note that the averaging error in D_0 is minimized via an iteration process, the
 21 details can be found in Rignot et al. (2008). Due to the lack of ice thickness information before
 22 2000, the reference D_0 in Rignot-08 has high uncertainty, especially in the northwest of the GrIS.

1 Another way to obtain historical discharge estimates is by using the presumed correlation between
 2 discharge and SMB or run-off (Rignot et al., 2008; Sasgen et al., 2012). The approach assumes that
 3 the anomaly of the discharge with respect to a reference SMB ($\delta D = \text{SMB}_0 - D$) is correlated with
 4 the anomaly of the 5-year averaging runoff with respect to a reference runoff ($\delta R = R - R_0$). Note
 5 that the lagging correlation is also discussed in Bamber et al. (2012) and Box and Colgan (2013).
 6 In this study we choose to use the runoff output from the RACMO2 model. We consider three
 7 estimates of D , i.e. by Rignot-08, Enderlin-14 and Andersen et al. (2015), based on different
 8 measurements of the ice thickness and flux velocity changes, integration areas (areas between the
 9 flux gate and the grounding line), SMB and ice storage corrections and whether the peripheral areas
 10 are included or not.. For the entire GrIS, we obtain a high correlation ($R^2 = \sim 0.86$), similar to the
 11 correlation found by Rignot et al. (2008), but the regional correlations are lower and vary from
 12 0.19 to 0.94. In this study we provide runoff-based estimates for D_0 only those ice sheet basins
 13 where the correlation between δD and δR is strong (Fig. 2). In DS7 and DS8, the discharge
 14 anomaly is obviously correlated with the runoff anomaly ($R^2 > 0.9$), while in other regions (i.e. in
 15 DS2, DS4, DS5 and DS6), the correlation is low ($R^2 < 0.5$). In DS3a, when we consider only the D
 16 estimates from Enderlin-2014 and Andersen-2015, the correlation increases to $R^2 = 0.72$. Note that
 17 the regions with high correlation are also those that have a large fraction of marine-terminating
 18 glaciers. We derive the linear relation between δD and δR for 8 major GrIS DS and calculate the
 19 regional annual δD from 1960 to 2013 using this linear relation.

20 Hereafter, the regional cumulative discharge anomaly (δD), which is derived from the RACMO2
 21 runoff, is denoted as D^R , while D^{D-08} and D^{D-14} refer to δD based on Rignot-08 and Enderlin-14,
 22 respectively. We compare D^R , D^{D-08} and D^{D-14} in Fig. 3 for the time interval 2000 to 2007, which
 23 is common to both D^{D-08} and D^{D-14} . In DS7, where $R^2 = 0.94$, D^{D-08} and D^{D-14} are similar, 20.1 ± 1.9

1 $\text{Gt}\cdot\text{yr}^{-1}$ and $17.6\pm 2.2 \text{ Gt}\cdot\text{yr}^{-1}$ respectively. However, in the same region, D^R is $8.9\pm 4.7 \text{ Gt}\cdot\text{yr}^{-1}$. The
 2 difference between the runoff-derived and flux gate D estimates may indicate that the reference D_0
 3 for this region should be $\sim 9 \text{ Gt}\cdot\text{yr}^{-1}$ lower than D_0 estimated by Rignot-08. A similar difference can
 4 be seen in DS4 where we obtain $36.2\pm 2.5 \text{ Gt}\cdot\text{yr}^{-1}$ for D^{D-14} and $37.9\pm 2.8 \text{ Gt}\cdot\text{yr}^{-1}$ for D^{D-08} , but D^R
 5 is $8.4\pm 3.3 \text{ Gt}\cdot\text{yr}^{-1}$. However, in DS4, D^R is probably not reliable as the runoff-to-discharge
 6 correlation is weak in this region ($R^2 = 0.38$). For the entire GrIS, the reference D_0 is $427\pm 30 \text{ Gt}$
 7 for D^{D-08} , and $414\pm 44 \text{ Gt}$ for D^{D-14} . When applying the runoff based interpolated D_0 only for DS1,
 8 DS3, DS7 and DS8, with the rest of DSs using D^{D-14} , D_0 becomes $410\pm 37 \text{ Gt}$, i.e. e all three
 9 versions of reference discharge agree within the uncertainties for the entire GrIS.

10 In order to evaluate the SMB_0 and D_0 used in this study, we compare the IOM regional mass balance
 11 in 8 major basins (interior and coastal regions are combined), and apply both Eq. (5) and Eq. (6).
 12 The latter equation relies on the determination of the SMB_0 and D_0 while Eq. (5) does not, so the
 13 comparison can provide an indication about the reliability of the SMB_0 and D_0 for some basins.
 14 For the application of equation (6) we use two methods. Method 2 uses D^{D-14} while method 3 uses
 15 D^R in DS1, 3, 7 and 8. As can be seen in Fig. 3, the three methods agree for the whole GrIS and for
 16 most of the basins within the uncertainties. In DS4, 7 and 8, however, methods 1 and 2 are
 17 significantly different, which may be caused by underestimated cumulative errors in Eq. (5) or less
 18 accurate reference SMB_0 and D_0 . This is further discussed in Sect. 4.3.

19 4.2. *Approximation errors*

20 In the solution of $\hat{\mathbf{x}}$, two types of errors occur: a) systematic errors are caused by measurement
 21 errors propagated through the least-squares approach and b) the additional error that is introduced
 22 when applying Eq. (9). For the type b) error, Bonin and Chamber (2013) show that Eq. (9) leaves

1 a noticeable difference between the approximation $\hat{\mathbf{x}}$ and the “truth” (a GrIS mass changes
 2 simulation), in particular in GrIS sub-regions, which we categorize as an error source, see also the
 3 discussion in Tiwari et al. (2009). Hereafter the type b) error is denoted as 'approximation error '
 4 or $\boldsymbol{\varepsilon}$. We estimate $\boldsymbol{\varepsilon}$ by using simulations of GrIS as \mathbf{x} , following Bonin and Chambers (2013) so
 5 that the approximation error becomes $\boldsymbol{\varepsilon} = \mathbf{x} - \hat{\mathbf{x}}$. The simulated regional mass changes on the
 6 mascons are $\mathbf{x} = [x_1, x_2, x_3, \dots, x_n]$, where n is the total number of mascons. We will show that
 7 there is a relation between $\hat{\mathbf{x}}$ and \mathbf{x} which can be used to correct for the approximation error.

8 The simulation model $\mathbf{y} = f(\theta, \lambda)$ is based on a 10 year linear trend (2003 to 2012) of mass changes
 9 of SMB and D estimates (see Sect. A3), with uncertainties of the simulation model written as
 10 $\boldsymbol{\sigma}(\theta, \lambda)$. We employ a Monte-Carlo approach to simulate a sample of 1000 randomly distributed
 11 observations, according to $\mathbf{y}_i' = \mathbf{y} + \mathbf{k}_i \boldsymbol{\sigma}$ with $\mathbf{k}_i = k_i(\theta, \lambda)$ a vector of random scaling factors
 12 varying from -1 to 1, and index i running from 1 to 1000. Hereby it is important to note that we
 13 assume that measurement errors do not exist (i.e. the simulation model is assumed to be reality).
 14 In addition we assume that the generated samples in the simulation ($\boldsymbol{\sigma}$) are normally distributed.

15 Next we apply Eq. (9) to yield approximated regional mass changes $\hat{\mathbf{x}} = [\hat{x}_i]$, in which i is the
 16 index of the mascons (see Fig. 1). The real regional mass change rate $\mathbf{x} = [x_i]$ are known from the
 17 simulation. As mentioned above, the difference between $\hat{\mathbf{x}}$ and \mathbf{x} equals the approximation error.
 18 In Fig. 4 we show that the x_i are linearly correlated with \hat{x}_i . By applying this correlation to the
 19 approximations derived from GRACE data, one can reduce the approximation errors in the GRACE
 20 based regional mass balance approximations.

21 The simulated trend in regional mass changes and the corresponding approximation are shown in
 22 Fig. 4. It can be noticed that the approximations are strongly correlated with the simulation in the

1 coastal regions over time with an average correlation coefficient $R^2 = 0.9$. This means that the
 2 approximated regional solutions are close to the simulation. The correlation in region DS1a is
 3 weaker (~ 0.6), which suggests that the approximation for region DS1a is influenced more by mass
 4 changes in neighbouring regions such as region DS8a. In the simulation the inter-region correlation
 5 between DS1a and DS8a is ~ -0.1 , while in the approximations, the correlation rises to ~ -0.5 . By
 6 comparison, another neighbour of DS8a, DS7a, has a very weak inter-region correlation with DS8a
 7 both in the simulation and in the approximation (~ 0.04). The inter-region correlation errors are
 8 systematic error resulting from to the least-squares inversion (Bonin and Chambers, 2013; Schrama
 9 and Wouters, 2011). Previous work shows that the regional approximation errors can be reduced
 10 when specifying constraints for the GrIS coastal and inland regions separately (Xu et al. 2015), but
 11 within the coastal region all the sub-DSs are constrained by the same prior variance in this study,
 12 thus the increase in correlation between DS1a and DS8a remains.

13 For the coastal regions, there is a linear relationship between the simulations \mathbf{x} and the
 14 approximation $\hat{\mathbf{x}}$, as can be seen in Fig. 4. We fit this relationship by $\mathbf{x} = \alpha_1 \hat{\mathbf{x}} + \alpha_0$, with a
 15 summary of α_1 and α_0 given in Table A1. The linear relationship between the simulated and the
 16 approximated regional mass changes rates is found to be stable; even when the simulation
 17 uncertainties are multiplied with a factor of 5 (light green marks in Fig. 4), the average regression
 18 parameters (α_1 and α_0) vary by less than $\sim 1\%$ for the coastal mascons. Therefore it is reasonable to
 19 assume that α_1 and α_0 reflect the relationship between the reality and the approximation, as
 20 derived from GRACE observations. When the vector of observations \mathbf{y} becomes the GRACE
 21 observations, the corresponding approximation $\hat{\mathbf{x}}$ can be improved by applying the linear
 22 relationship to. We will show that this correction yields a better agreement between GRACE and
 23 the IOM in Sect. 4.3.

1 Contrary to the coastal regions, the linear relation between \mathbf{x} and $\hat{\mathbf{x}}$ is weak in the interior regions,
2 where the mean correlation coefficient is ~ 0.2 . This may be because interior regions show smaller
3 mass change rates than the coastal regions. For simulations created within a 1σ range, the highest
4 correlation coefficient is only 0.47 for DS7b. The strong constraint used for these regions, i.e. a
5 prior variance of 0.1 m^2 , may cause the approximation to be more determined by this constraint
6 than the simulation. However, if we apply a weaker constraint, i.e. $\lambda = 10^6$, the correlation
7 coefficients between \mathbf{x} and $\hat{\mathbf{x}}$ in these regions remain below 0.5. This means that correcting the
8 approximation errors using the same method as for the coastal regions may create larger
9 uncertainties. Following Bonin and Chambers (2014), we choose to include the approximation
10 errors in the uncertainties but only for the interior regions. The uncertainties are shown in Table
11 A2.

12 4.3. *Results and discussions*

13 We compared the regional mass changing rate from GRACE with the IOM (Fig. 5) before and after
14 applying the approximation error correction to GRACE and with different discharge estimations
15 implemented by the IOM, separately for coastal and interior regions. For the coastal regions, we
16 find that the correction of the approximation errors in the GRACE solutions shifts the mass
17 distributions between adjacent mascons. For instance, the corrected mass loss rate in DS3a
18 increases by $10 \text{ Gt}\cdot\text{yr}^{-1}$ while it reduces the mass loss rate in the adjacent region DS4a by $15 \text{ Gt}\cdot\text{yr}^{-1}$.
19 In mascon DS5a, DS6a and DS7a, the combined mass change rate is $-107 \pm 8 \text{ Gt}\cdot\text{yr}^{-1}$ before
20 correcting and $-106 \pm 8 \text{ Gt}\cdot\text{yr}^{-1}$ after correcting for regional approximation errors. In mascon DS6a
21 correcting for the approximation error causes a mass loss increase of $13 \text{ Gt}\cdot\text{yr}^{-1}$.

1 In the comparison we only consider TMB from the IOM in order to reduce the influence of the
2 individual uncertainties in SMB and D. We obtain two IOM solutions, using the reference D_0 by
3 Rignot-08 (method 2) and the interpolated discharges based on RACMO2 runoff (method 3). In
4 mascon DS1a and DS3a, we obtain lower discharge changes rate from method 3 than from method
5 2. In mascon DS7a, which includes Jakobshavn glacier, method 3 results in smaller mass changes
6 than method 2.

7 Fig. 5 shows that agreement between GRACE and IOM improves after correcting the GRACE
8 approximation errors and applying the runoff based discharge estimations in mascon DS3a, DS5a,
9 DS6a and DS7a. The difference between GRACE and IOM estimates is also reduced in DS1a and
10 DS2a, where the remaining difference falls within the uncertainty margins. The corrected GRACE
11 solution in DS4a is only $\sim 3 \text{ Gt}\cdot\text{yr}^{-1}$ lower than the IOM solution while it was $10 \text{ Gt}\cdot\text{yr}^{-1}$ higher
12 before correction. However, regardless of correcting the approximation errors, the GRACE inferred
13 regional mass balance agrees with IOM mass balance in DS4a due to the large uncertainties in the
14 GRACE solution and the RACMO2 model there, i.e. $\pm 17 \text{ Gt}\cdot\text{yr}^{-1}$ (see Table A2). From Fig. 5 we
15 can also make some inferences about the effect of using different methods to estimate the reference
16 discharge. Only in mascon DS8a, IOM and GRACE do not agree within the uncertainties. Previous
17 studies, e.g. Bolch et al. (2013) and Gardner et al. (2013), show that approximately $40 \text{ Gt}\cdot\text{yr}^{-1}$ mass
18 losses are from the peripheral glaciers. Yet, these portion of mass losses are not considered in our
19 IOM solution. However, given the relationship we found in our discharge data between glacier
20 width and area for the ice sheet's marine-terminating glaciers, we suspect the discharge from these
21 glaciers is quite small and the regional mass changes in these glacier areas are dominated by
22 changes in SMB. the GRACE-IOM difference will likely be on the order of several $\text{Gt}\cdot\text{yr}^{-1}$ due to

1 the exclusion of discharge from peripheral marine-terminating glaciers and ice caps as long as we
2 consider the SMB for the whole of Greenland, not just the ice sheet.

3 For the regions above 2000 m altitude, GRACE inferred regional mass change rates agree with the
4 RACMO2 SMB estimations within uncertainties (see Fig. 5). A noticeable mass increase appears
5 in both GRACE and IOM solutions in mascon 2b (northeast interior). A second observation is that
6 in the IOM, the runoff dominates the regional mass balance on the edge of the southern GrIS
7 interior resulting in mass loss of $-8 \text{ Gt}\cdot\text{yr}^{-1}$. The overall IOM uncertainties in the coastal regions
8 are mainly influenced by the uncertainties in SMB and D estimates, meanwhile applying the
9 assumptions on the flux across the 2000m contour (F^{II}) contributes additional uncertainties in the
10 GrIS interior regions. In the GRACE solution, the uncertainties are due to the errors in the GRACE
11 coefficients which is not dependent on the altitude, therefore the uncertainty level is similar to the
12 coastal regions.

13 We also compare our GRACE and IOM solutions to other studies based on GRACE, IOM and
14 ICESat altimetry, as shown in Table 1. All listed GRACE solutions agree within uncertainty levels
15 in DS1, DS2, DS3, DS5 and DS8. In line with some of the referenced studies, we combine DS6
16 and DS7. We find a larger rate of mass loss in this area compared to other studies (i.e. -87 ± 10
17 $\text{Gt}\cdot\text{yr}^{-1}$) because a longer time interval is considered in this study and mass loss accelerates by \sim
18 $16 \text{ Gt}\cdot\text{yr}^{-2}$ over the entire period according to our solution. After accounting for this acceleration,
19 all GRACE solutions become similar in this combined region.

20 In the southeast region DS4, the regional acceleration of mass loss is negligible ($\sim -0.1 \text{ Gt}\cdot\text{yr}^{-2}$).
21 When comparing different GRACE solutions, the mass loss rate in DS4 ranges from $-28 \pm 7 \text{ Gt}\cdot\text{yr}^{-1}$
22 to $-51 \pm 6 \text{ Gt}\cdot\text{yr}^{-1}$. It suggests that a large approximation error, which is associated with different

1 approximation approaches, is likely present in this region in the GRACE solution. As shown in Fig.
2 5, the regional mass change is reduced by 29% in this region after applying the correction.

3 The IOM is also relatively uncertain in DS4 (Sasgen et al., 2012). Even if the mass changes rates
4 are very different between GRACE and IOM in this region, agreement is obtained within the large
5 uncertainties. For ICESat-based mass loss estimates, the retrieved long-term mass loss can be very
6 different, e.g. -75 ± 2 Gt·yr⁻¹ by Zwally et al. (2011) compared to -40 ± 18 Gt·yr⁻¹ by Sørensen et al.
7 (2011). This may be explained by the complicated regional ice surface geometry in the coastal
8 areas (Zwally et al., 2011), or uncertainty resulting from the conversion of height changes to mass
9 changes, e.g. different firn corrections and density conversions.

10 Another area where GRACE and IOM do not agree is the northwest (region DS8). In this region,
11 mass loss is accelerating by -3 ± 0.4 Gt·yr⁻² and -5 ± 1 Gt·yr⁻² according to our GRACE solution and
12 IOM solution respectively. If we extend the time interval to 2013, we find that GRACE and ICESat
13 solutions suggest a similar mass loss rate (see Table 1). Moreover, if we determine the mass change
14 rates for the time interval from 2007 – 2011, the rate is -57 ± 6 Gt·yr⁻¹ (GRACE) and -49 ± 11 Gt·yr⁻¹
15 (IOM), and both agree with the rate from Andersen et al. (2015). We have reduced the
16 approximation error in the GRACE solution for this region, although by a small amount (-2.3
17 Gt·yr⁻¹).

18 There is another way to judge whether approximation errors exist in GRACE. When the
19 approximation errors exist for one region, the error is likely of similar magnitude but of opposite
20 sign in neighbouring regions, which we refer to as negative correlation errors (Xu et al. 2015). In
21 this study, the adjacent regions of DS8 are DS1, DS7 and Ellesmere Island (northern Canadian
22 Arctic) and in all three neighbour regions, the mass changes rate between GRACE and IOM

1 solutions are similar, see Fig. 5. Note that Ellesmere Island is not shown in this figure; the
2 corresponding changes rates are $-36 \pm 7 \text{ Gt}\cdot\text{yr}^{-1}$ and $-29.4 \pm 3 \text{ Gt}\cdot\text{yr}^{-1}$ in IOM and GRACE solutions
3 respectively. This suggests that the difference of the regional mass changes in DS8 is not due to
4 the approximation error in the GRACE solution because there is no negative correlation between
5 adjacent areas. The uncertainties of the GIA effect are included as part of the uncertainties of the
6 GRACE solution for this region as well (see Table A3), but adding these still cannot bridge the gap
7 between GRACE and IOM. The ICESat-based mass change estimate by Kjeldsen et al. (2013)
8 yields a mass loss rates of $55 \pm 8.4 \text{ Gt}\cdot\text{yr}^{-1}$ from 2003 to 2010, which is consistent with the GRACE
9 solution in this study. All evidence combined indicates that the IOM method underestimates the
10 mass loss rate in this basin by $\sim -15 \text{ Gt}\cdot\text{yr}^{-1}$. In Sasgen et al. (2012), the discharge estimations from
11 Rignot-08 are used, in which a portion of DS8 was un-surveyed, to which they ascribed the
12 difference between GRACE and IOM ($24 \pm 13 \text{ Gt}\cdot\text{yr}^{-1}$). In this study, the discharge estimation from
13 Enderlin et al. (2014) covers the entire glacier area in this region, but only for the years after 2000.
14 Therefore, despite observations of relatively stable terminus positions for the majority of the
15 marine-terminating glaciers in northwest Greenland between 1985-2000 (Howat and Eddy, 2011),
16 we hypothesize that the estimated reference discharge over-estimates the regional D_0 . Deriving D_0
17 from D-14 involved the assumption that D from 1990 to 2000 follows Rignot-08, which contains
18 high regional uncertainties. On the other hand, if we use the runoff-based estimate of D_0 ,
19 uncertainties are influenced by the uncertainty of the RACMO2 model. The SMB inter-comparison
20 study of Vernon et al. (2013) shows that the 1961-1990 reference SMB_0 of RACMO2 model is
21 larger than some other SMB models, e.g. MAR or PMM5. It is interesting to see that when the
22 cumulative TMB is calculated independently from the reference SMB_0 and D_0 (using Eq (5),
23 method 1), the mass changes rate agrees with the GRACE mass balance in this region within

1 uncertainties. This indicates that modelled SMB (as well as SMB_0) could have uncertainties that
2 are larger than 18%.

3 **5 Conclusions**

4 In this study, we implement a simulation of GrIS mass changes and show that the approximation
5 errors caused by the Least Squares inversion approach can be quantified and furthermore be
6 reduced in the GRACE solution. For using the IOM, we apply an improved reference discharge
7 estimate that agrees better with other independent estimates in most basins. We show that the
8 regional differences between our GRACE and IOM solutions are reduced and agree within the
9 calculated confidence intervals. This is confirmed by an inter-comparison with ICESat based
10 regional mass change rates. In the southeast, the corrections for the approximation errors in
11 GRACE are especially important. We find that the IOM solutions underestimate mass loss in the
12 northwest compared to GRACE and ICESAT solutions, which we attribute to incorrect estimates
13 in reference D and/or SMB used to construct the IOM estimates. For the whole GrIS and
14 considering the early half of the comparison time window, we find a $208 \pm 18 \text{ Gt}\cdot\text{yr}^{-1}$ mass loss rate
15 for the period 2003 to 2008 from the GRACE solution, while the IOM solution shows a mass loss
16 rate of $195 \pm 25 \text{ Gt}\cdot\text{yr}^{-1}$. The loss rates increase by $\sim 67\%$ and $\sim 85\%$ in 2009-2014 in the GRACE
17 and IOM solutions, respectively. The 10-year acceleration in the GRACE data is $-25 \pm 8 \text{ Gt}\cdot\text{yr}^{-2}$,
18 consistent with the IOM solution, $-26 \pm 12 \text{ Gt}\cdot\text{yr}^{-2}$.

19 *Acknowledgements.* This research is funded by means of scholarship GO-AO/27 provided by the
20 Netherlands Organization of Scientific Research, NWO. We are grateful to Ian Joughin for the
21 suggestions of estimating the ice flux at high elevation. Furthermore the authors acknowledge the
22 thoughtful comments by Etienne Berthier and three anonymous referees of this manuscript.

1 **Appendix A**

2 **A1: Reference discharge based on the pre-1960 discharge estimations**

3 The GrIS ice discharge D was distributed into 34 glaciers by Rignot et al. (2008), denoted by D -
 4 08. The reference discharge D_{0-08} is taken as the discharge estimate for the year of 1996. We label
 5 the discharge in 1996 and 2000 as D_{0-08} and $D_{2000-08}$, respectively. The deviations between D_{0-08} -
 6 08 and $D_{2000-08}$ are due to the discharge changes in the late 1990s (Enderlin et al., 2014). Similarly,
 7 we define Enderlin-14 as D -14, with the time series starting from the year of 2000 ($D_{2000-14}$). In
 8 order to estimate the reference discharge D_{0-14} , we find scaling factors between D_{0-08} and $D_{2000-08}$ -
 9 08 and scale the $D_{2000-14}$ to yield the estimation of D_{0-14} . We estimate the uncertainties of
 10 estimated D_{0-14} via 500 pairs of randomly generated \tilde{D}_{0-08} , $\tilde{D}_{2000-08}$ and $\tilde{D}_{2000-14}$, following from
 11 a normal distribution $N(D, \sigma_D)$, in which σ_D is the error in the discharge estimations. For the entire
 12 GrIS, we find that the interpolated $D_{14_0} = 413.8 \pm 31.6$ Gt, similar to previous studies (Sasgen et al.,
 13 2012; van den Broeke et al., 2009).

14 **A2 Approximation error correction**

15 In order to determine the linear relationship between the simulated regional mass balances with the
 16 associated approximations after applying the Least Squares inversion, the linear fitting parameters
 17 k_0 and k_1 are calculated for different simulation error levels, the values of which are shown in Table
 18 A1. The values of k_0 and k_1 and their uncertainties vary slightly in all coastal regions. In order to
 19 determine one value for k_0 and k_1 , we assume the k_0 and k_1 follow a normal distribution in each
 20 region and draw 1000 random samples for each error level. Then we combine all the samples and
 21 fit into another normal distribution from which the k_0 and k_1 are determined for each region (see
 22 the Table A1).

1 **A 3 The GrIS simulation**

2 The GrIS monthly mass balance simulations that will be used in section 4.2 are based on the
3 RACMO2 model and the discharges estimates from Enderlin et al., (2014). Note that the discharge
4 estimates are given the form of lumped mass change for 178 different geographical locations. To
5 get SMB and D estimates for each basin we sum the discharges for all glaciers or the gridded SMB
6 values within each basin, respectively. We interpolate SMB and D onto a gridded map of EWH
7 with a resolution of 1 arc degree for the GrIS and surrounding areas. To account for leakage from
8 outside the GrIS, as occurs in GRACE, we apply the annual mass changes estimates from Schrama
9 et al. (2014) for all the major glacier areas (GrIS excluded). We convolve the gridded mass
10 distribution over the Earth's surface and obtain the potential coefficients in response to this
11 distribution up to d/o 60. Noise in the monthly GRACE coefficients manifests mainly as north-
12 south stripes in the spatial domain (Swenson and Wahr, 2006). In order to mimic this error in the
13 simulation, we add randomly generated noise as described in Bonin and Chambers (2013) to the
14 potential coefficients. The simulation model was discussed in details in Xu et al., (2015). Note that
15 for this study we focus on the discussion of long term linear trend, thus the linear trend of the
16 monthly simulation is used as the simulation model for later use.

17 **A 4 Uncertainty estimations**

18 A summary of the uncertainties in the regional mass balance (linear trend) is shown in Table A2.
19 In our GRACE inferred mass balance, the uncertainties are associated with the standard deviations
20 of the CSR RL05 GRACE spherical harmonics coefficients (including the standard deviations of
21 the external degree $l = 1$ and 2 coefficients), the variations of the regional mass changes due to
22 different GIA models and the uncertainties due to the corrections of the systematic error in the

1 least-squares inversion solutions. The uncertainties of the IOM inferred mass balance consist of
2 the uncertainties of the 1960 – 1990 reference in SMB_0 and in D_0 and 2b) the systematic error in
3 the SMB (RACMO2) and 2c) the errors in the yearly D estimations (Enderlin 2014 and Rignot
4 2008).

5 **A 5 Selection of the GIA model for GrIS regions.**

6 We apply the GIA correction to the GRACE data using 11 different GIA models before estimating
7 the associated regional mass changes in 20 GrIS and surrounding Arctic regions (see the mascon
8 definition in Sect. 3). After comparing with one solution without applying GIA correction, we
9 assume the differences are the regional GIA effects. In addition to Paulson-07 GIA model, we use
10 a GIA model with lateral changes in viscosity and the ICE-5G loading history (van der Wal et al.
11 2013).

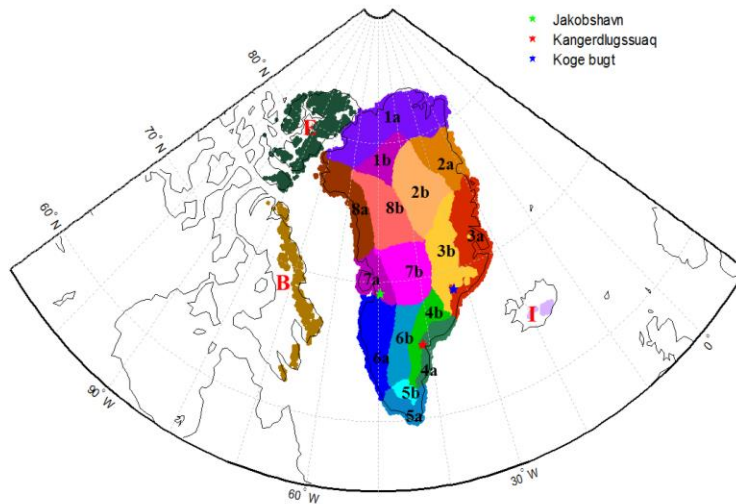
12 Moreover, we use 8 different GIA models based on the ice history model from Simpson et al.
13 (2009), provided by Glenn Milne within the scope of the IMBIE project. The upper mantle
14 viscosity ranges from 0.3×10^{21} to 1×10^{21} Pa·s and the lower mantle viscosity ranges from 1×10^{21}
15 to 10×10^{21} Pa·s. The thickness of the lithosphere is assumed to be 96 km or 120 km.

16 In Table A3, the GIA related mass changes can vary from $-7 \text{ Gt}\cdot\text{yr}^{-1}$ to $10 \text{ Gt}\cdot\text{yr}^{-1}$ for the entire
17 GrIS. A positive GIA effect appears in the northern GrIS while in the south and southwest GrIS,
18 (DS5a to DS7a) negative GIA signals prevail.

19 In order to quantify the uncertainties of the regional GIA in the Paulson-07, since it is the GIA
20 model we used to derive our GRACE solution, we estimate the standard deviation of all models
21 with respect to Paulson-07. The uncertainties are summarized in Table A2.

1 Figures

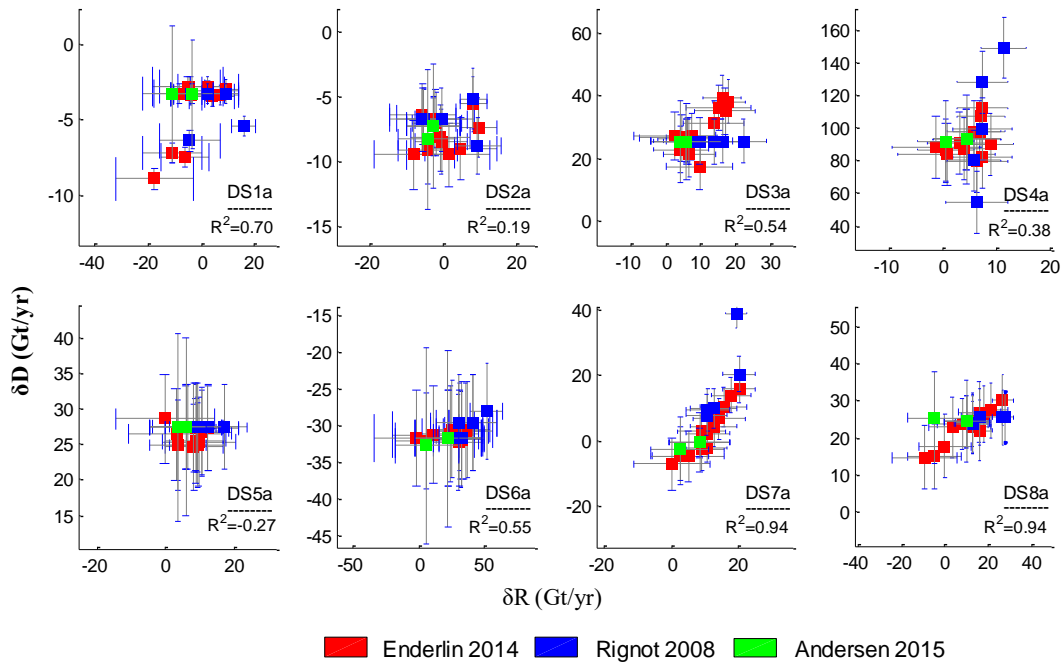
2



3

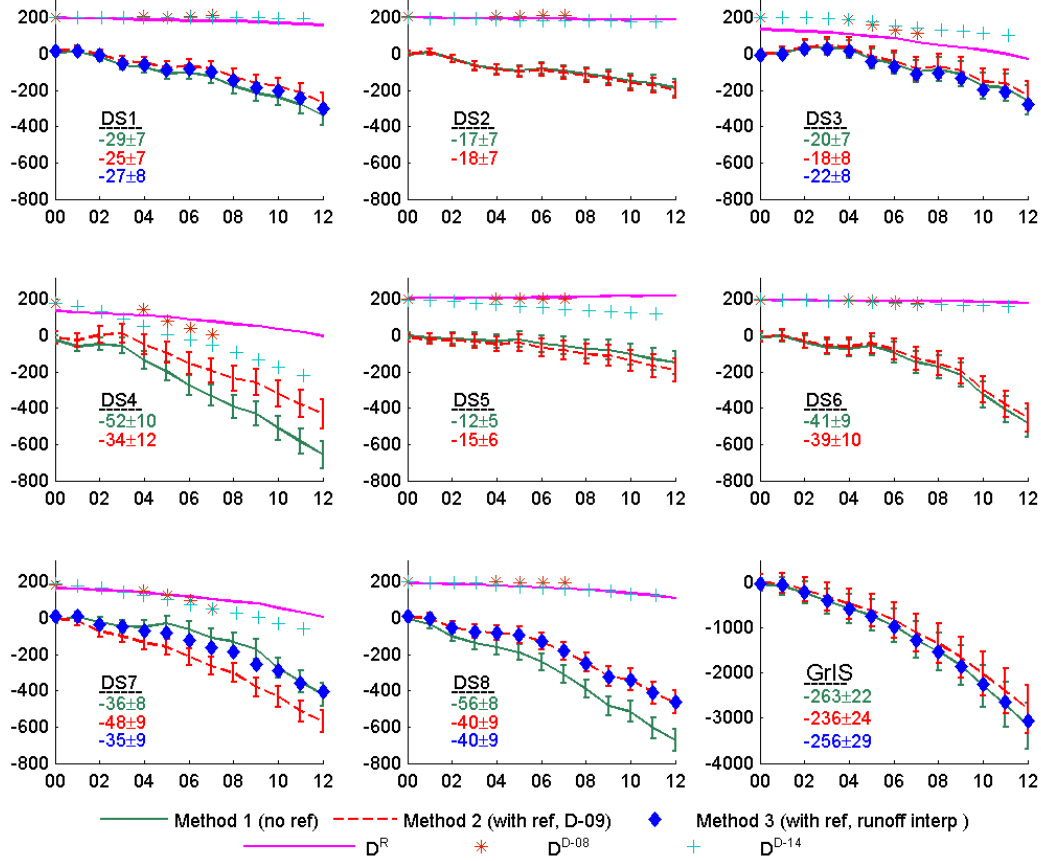
4 **Figure 1. The GrIS mascon layout, based on the basin definition by Zwally (2012). The**
 5 **mascon with the same digits refer to a region belonging to the same drainage system. The**
 6 **characters “a” and “b” indicate the GrIS margin (<2000m) and GrIS interior (≥ 2000 m),**
 7 **respectively. There are 16 GrIS mascons and 4 neighbouring Arctic mascons. The location of**
 8 **the three largest discharge outlets are marked with a star, i.e. Jakobshavn (green),**
 9 **Kangerdlugssuaq (red) and Koge Bugt (blue) glaciers. The glacier area is defined in the**
 10 **RACMO2 model.**

11

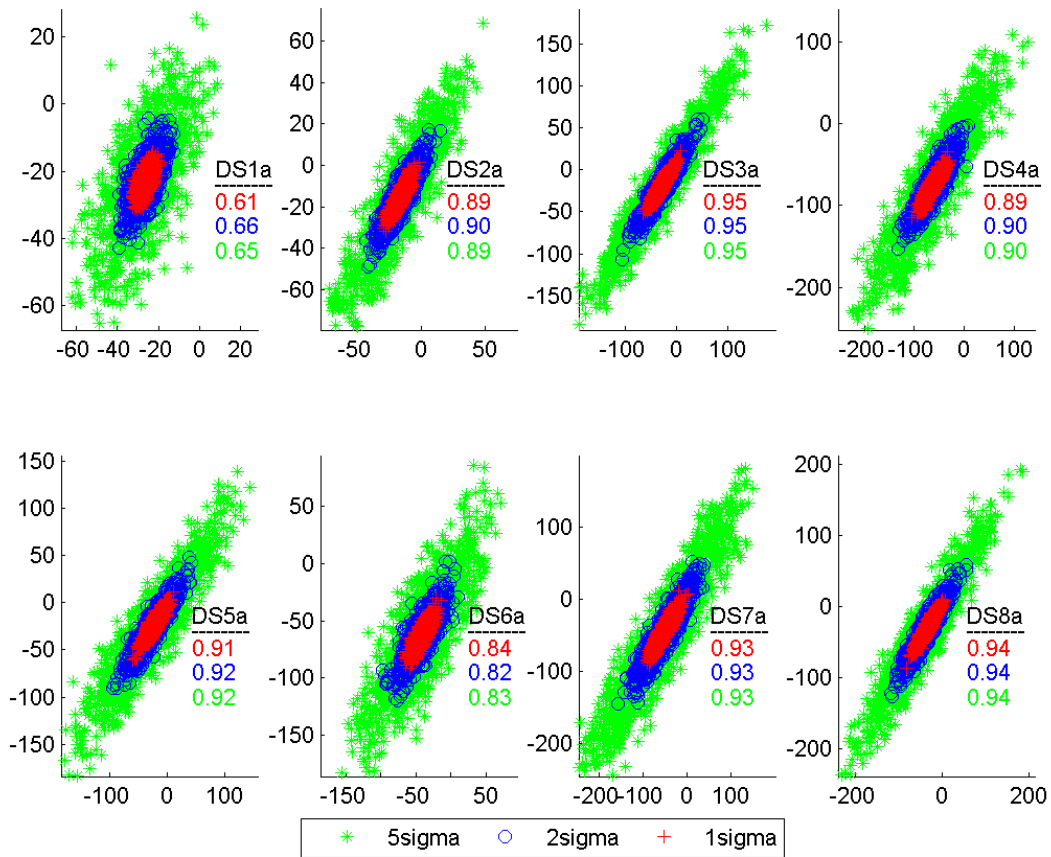


1

2 **Figure 2. Correlation between the anomaly of the discharge δD with respect to a reference**
 3 **SMB (y-axis) and the 5-year averaging runoff δR (x-axis) in GrIS regions. The symbols with**
 4 **different colours refer to different estimates of D . The grey bars for both δD and δR indicate**
 5 **the errors. The correlation coefficients R^2 are also shown in each plot.**



1
 2 **Figure 3.** The comparison between cumulative TMB (2000-2012) obtained with three
 3 different methods. Method 1, using no reference TMB, is shown with a green curve. The
 4 cumulative TMB obtained with a 1960 – 1990 reference TMB is shown with a red curve
 5 (method 2) and blue markers (method 3). Method 2 and Method 3 compute the reference
 6 discharge in a different way. In method 2, D_0 is based on the estimation from Rignot-08 and
 7 for the years after 2000, the estimation from D-14 is used (D^{D-14}). Method 3 interpolates the
 8 reference discharge using the modelled runoff data (only in DS1, 3, 7 and 8), denoted as D^R .
 9 D^{D-08} refers to the discharge changes by D-08. All the discharges are shifted upward by 200
 10 Gt for visualization purposes. The numbers in each plot indicate the annual TMB change
 11 rates with the unit Gt·yr⁻¹. The x-axis shows the last two digits of the years from 2000 to 2012.



1

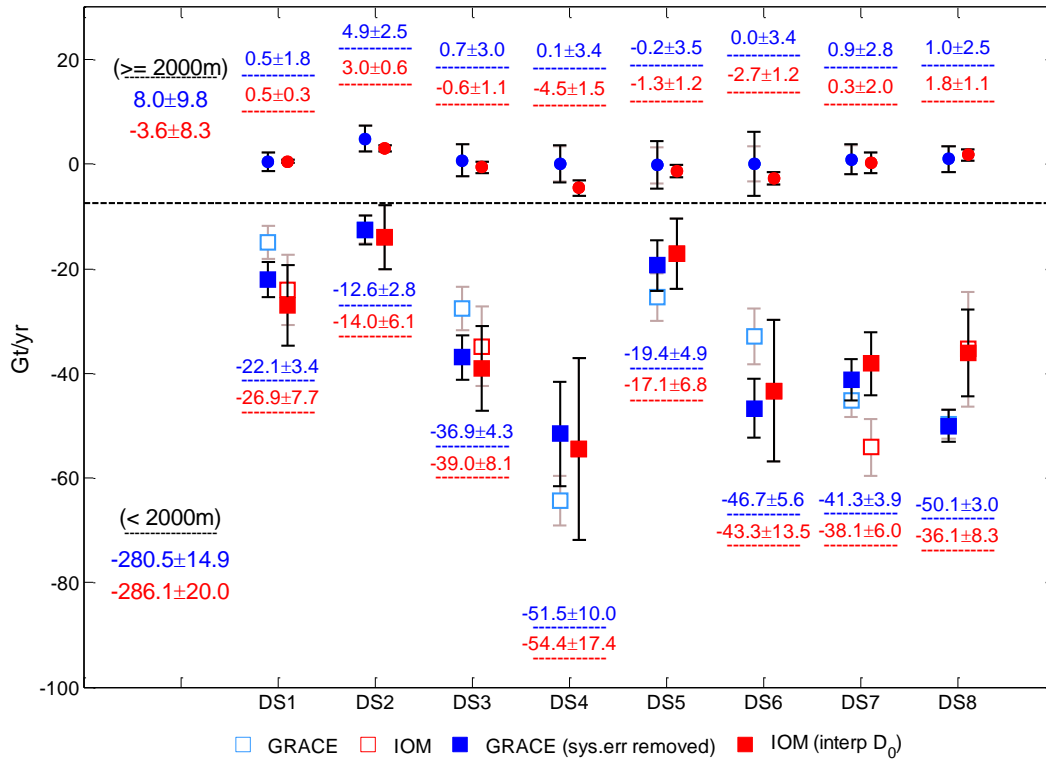
2 **Figure 4. Correlation between the linear trend in the simulations x' (y-axis) and the**

3 **corresponding approximation \hat{x}' (x-axis). The unit is in $\text{Gt}\cdot\text{yr}^{-1}$. The colours are associated**

4 **with the changing range of x' for a standard deviation going from 1σ to 5σ . The numbers**

5 **refer to the R^2 coefficient for three different σ .**

6



1

2 **Figure 5. Comparison of the regional mass changes rate between the GRACE solution and**

3 **the IOM solutions. Each column refers to one complete basin according to Zwally (2012).**

4 **The regional mass change rates from GRACE before correcting for the approximation error,**

5 **are represented by the light blue hollow squares; the filled dark blue squares indicate the**

6 **mass change rates after implementing the correction. The numbers show the mass changes**

7 **rate in blue and red colours which indicate the GRACE solution and IOM solution**

8 **respectively. The dashed line separates the solutions from the interior regions (above the**

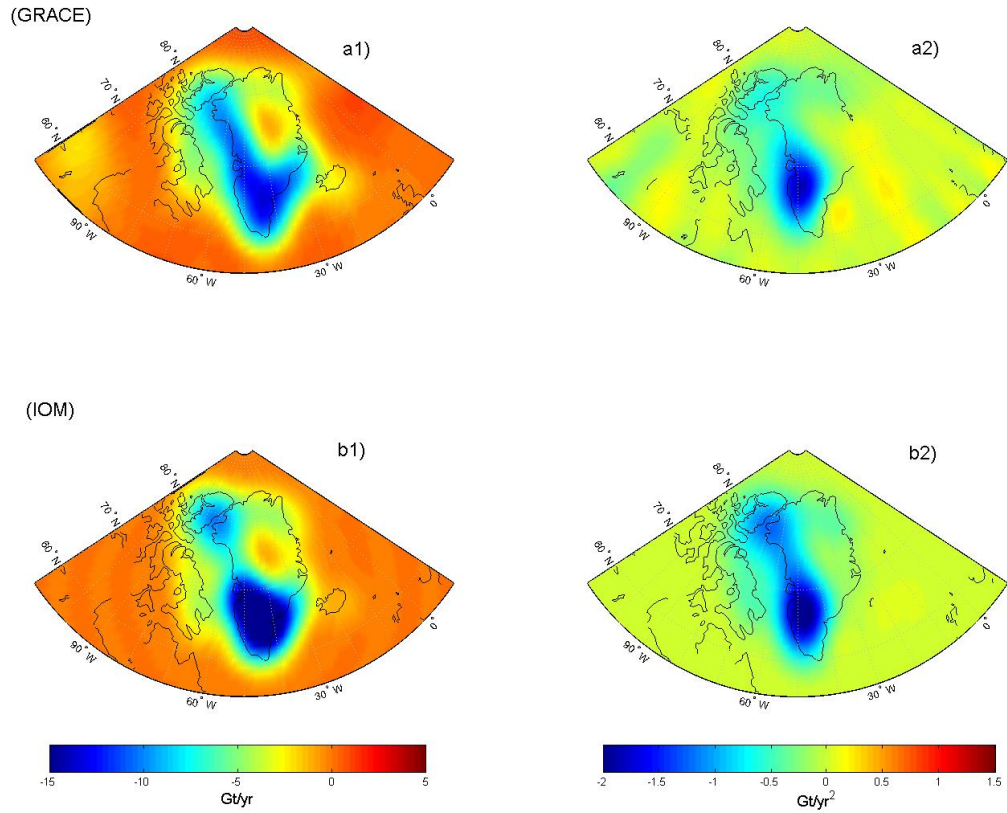
9 **dashed line) from the coastal regions (below the dashed line). The error bars are estimated**

10 **in Sect. A4.**

11

12

1



2

3 **Figure A1. The Equivalent Water Thickness of the linear trend (a1) and accelerations (a2) in**
 4 **CSR release 5 level 2 GRACE data. The linear trend (b1) and the accelerations (b2) of the**
 5 **IOM solution in EWH. The time interval is from Jan 2003 to Jan 2012. The Gaussian filter**
 6 **halfwidth in all plots is $r_{1/2}=300$ km.**

7

8

1 **Tables:**

2 **Table 1: Linear trends in the mass changes in GrIS regions based on satellite gravity data**
3 **(GRACE), IOM output and altimetry data (ICESat). The unit is $\text{Gt}\cdot\text{yr}^{-1}$. The studies are:**
4 **Zwally et al., 2011; Sasgen et al., 2012; Barletta et al., 2013; Colgan et al., 2013; Groh et al.,**
5 **2014; Andersen et al., 2015; Sørensen et al., 2011.**

Basin	DS1	DS2	DS3	DS4	DS5	DS6	DS7	DS8
	GRACE							
This study (2003-2013)	-22±4	-8±4	-36±5	-51±6	-20±6	-47±8	-40±5	-50±4
Colgan (2003 - 2010)	-21±6	1±6	-47±13	-28±7	-24±4	-33±7	-23±9	-42±12
Sasgen (2003 - 2010)	-16±5	-12±5	-38±6	-42±6	-24±6		-56±7	-53±7
Barletta (2003-2012)	-17±2	-12±2	-36±4	-35±3	-23±2		-66±4	-44±4
	IOM							
This study (2003 - 2013)	-26±8	-10±6	-39±8	-59±18	-18±7	-46±14	-38±6	-35±8
Andersen (2007 - 2011)	-17±5	-13±6		-38±29	-20±9	-53±13	-53±17	-58±14
Sasgen (2003-2010)	-20±4	-16±5	-31±8	-66±21	-20±7		-66±20	-26±12
	ICESat							
Zwally -11 (2003-2007)	1±0	13±0	-51±1	-75±2	-10±0	-4±0	-14±0	-33±1
Sørensen (2003 - 2009)	-16±1	-16±3	-40±18	-43±11	-26±5		-51±7	-53±3

6

7

1 **Table A1: The linear fit parameters k_0 and k_1 describing the relationship between the**
 2 **regional simulated mass balance and the approximations obtained after the inversion**
 3 **procedure as applied to GRACE data of the coastal regions. For the interior GrIS regions,**
 4 **we show the approximation errors as additional uncertainties.**

mascon (< 2000m)	DS1a	DS2a	DS3a	DS4a	DS5a	DS6a	DS7a	DS8a
α_0 (Gt)	-10.93 \pm 1.46	-0.64 \pm 0.54	6.82 \pm 1.47	-14.90 \pm 1.54	-1.86 \pm 1.61	-17.15 \pm 1.54	2.54 \pm 2.23	0.28 \pm 1.02
α_1	0.85 \pm 0.03	1.02 \pm 0.02	0.95 \pm 0.01	0.96 \pm 0.02	0.90 \pm 0.01	0.90 \pm 0.02	0.97 \pm 0.01	1.00 \pm 0.01
mascon (\geq 2000m)	DS1b	DS2b	DS3b	DS4b	DS5b	DS6b	DS7b	DS8b
uncertainty (Gt \cdot yr $^{-1}$)	0.28	0.35	0.45	0.6	2.88	5.1	0.67	0.65

5

6

1 **Table A2: The uncertainties associated with the regional mass changes rate. For the GRACE**
2 **inferred regional solutions, “coef.std” refers to the errors due to the standard deviations in**
3 **the CSR RL05 spherical coefficients, “GIA” refers to the errors obtained from comparing 11**
4 **GIA models. Note that the GIA uncertainties in the interior GrIS are all close to 0 thus they**
5 **are neglected. In the column with the header “Cor” we show the uncertainties which are**
6 **caused by the approximation error correction. For SMB and D trend estimations, the**
7 **uncertainties consist of the reference SMB₀ and D₀ error (“SMB₀” and “D₀”) and the**
8 **systematic errors in RACMO2 model and in the discharge estimations (“sys”). The column**
9 **labeled with “Cum. Uncer” refers to uncertainties using the assumptions 1) and 2), see the**
10 **details in Sect. 3.2. The highlighted columns show the total uncertainties of the linear fit of**
11 **the GRACE and IOM mass balances.**

Mascon	GRACE				RACMO2 (SMB)			Discharge (D)			Cum.Uncer	IOM
	coef.std(1a)	GIA (2a)	Cor (3a)	Total	SMB ₀ (1b)	Sys (2b)	Total	D ₀ (1c)	Sys (2c)	Total	Apply assum. 1) and 2)	SMB-D
DS1a	1.9	3.9	1.6	3.4	1.9	7.2	7.6	0.8	0	0.8	1.1	7.7
DS2a	2.1	2.2	0.6	2.8	1.6	5.8	6	1.1	0.3	1.1	2.9	6.8
DS3a	3.2	3	1.5	4.3	3.6	6.8	7.8	2	1	2.2	2.1	8.4
DS4a	3.8	2.6	8.8	10	8.6	10.6	17.1	3.1	1.4	3.4	1.6	17.5
DS5a	4.4	0.2	1.7	4.9	3.9	5.2	6.7	1.1	0.7	1.2	0.8	6.9
DS6a	3.7	0.8	1.7	5.6	4.7	12.5	13.4	0.6	0.3	0.6	1.4	13.5
DS7a	3	0.5	2.2	3.9	2	4.9	5.4	2	1.5	2.5	4.9	7.7
DS8a	2.4	3.7	1.1	4.5	3.3	7.7	8.3	2.1	1.1	2.4	2.3	8.9
Coastal	9	7.3	4.5	14.9	12.1	22.6	27.7	4.9	2.7	5.5	15.4	32.2
DS1b	1.8		0.3	1.8	0.3	0.1	0.3				1.1	1.1
DS2b	2.4		0.4	2.4	0.6	0.2	0.6				2.9	3.0
DS3b	3		0.5	3	1	0.3	1.1				2.1	2.4
DS4b	3.4		0.6	3.5	1.5	0.3	1.5				1.6	2.2
DS5b	3.5		2.9	4.5	1.1	0.3	1.2				0.8	1.4
DS6b	3.4		5.1	6.1	1.2	0.4	1.2				1.4	1.8
DS7b	2.8		0.7	2.9	1.8	0.6	2				4.9	5.3
DS8b	2.4		0.7	2.5	0.9	0.4	1.1				2.3	2.5
interior	7.8		6	9.8	8.1	1.7	8.3				15.4	17.5
GrIS	11.9	7.3	7.5	17.8	14.5	22.7	28.9	4.9	2.7	5.5	0	29.4

1 **Table A3: The GIA effects on mass balance in different GrIS regions based on 11 different**
 2 **GIA models. The unit is $\text{Gt}\cdot\text{yr}^{-1}$. For the GIA models using Simpson’s ice history model, the**
 3 **column headers are in the form of “ $xpab$ ”, where the x value refers to the lithosphere**
 4 **thickness (km), and a and b represent the viscosity of the upper and lower mantle, in 10^{20} and**
 5 **10^{21} Pa·s respectively.**

ICE model	ICE-5G	Wouter van der Wal		Simpson							
Mascon	Paulson-07	heatflow	seismic	96p32	96p55	96p58	96p85	96p510	120p51	120p81	120p11
DS1a	4	5	2	1	-1	-1	-1	0	3	4	4
DS2a	3	1	1	1	1	1	2	2	2	3	3
DS3a	0	2	-1	1	-1	-2	-1	-1	2	3	3
DS4a	0	3	1	-1	0	0	1	1	1	3	4
DS5a	-3	-1	0	-5	-8	-7	-7	-7	-4	-4	-5
DS6a	-2	1	2	-5	-2	-2	1	-2	-3	-1	0
DS7a	-3	0	0	-1	-5	-5	-6	-5	-2	-2	-3
DS8a	-1	-1	0	1	-1	-2	-2	-2	-1	-2	-2
Ellesmere	7	4	4	1	2	3	4	3	4	5	6
Baffin	12	-3	6	10	12	12	12	13	1	0	-1
Iceland	-1	0	-1	-1	-3	-3	-3	-3	0	0	-1
Svalbard	2	0	2	2	3	4	3	5	0	0	0

6

7

References

- 1
2 Andersen, M. L., Stenseng, L., Skourup, H., Colgan, W., Khan, S. A., Kristensen, S. S., Andersen, S. B.,
3 Box, J. E., Ahlstrøm, A. P., Fettweis, X., and Forsberg, R.: Basin-scale partitioning of Greenland ice sheet
4 mass balance components (2007–2011), *Earth Planet SC Lett*, 409, 89-95, 2015.
5
6 Bales, R. C., Guo, Q., Shen, D., McConnell, J. R., Du, G., Burkhart, J. F., Spikes, V. B., Hanna, E., and
7 Cappelen, J.: Annual accumulation for Greenland updated using ice core data developed during 2000–2006
8 and analysis of daily coastal meteorological data, *J Geophys Res-Atmos* (1984–2012), 114, 2009.
9
10 Bamber, J., van den Broeke, M., Ettema, J., Lenaerts, J., and Rignot, E.: Recent large increases in freshwater
11 fluxes from Greenland into the North Atlantic, *Geophys Res Lett*, 39, L19501, DOI:
12 10.1029/2012GL052552, 2012.
13
14 Barletta, V. R., Sørensen, L. S., and Forsberg, R.: Scatter of mass changes estimates at basin scale for
15 Greenland and Antarctica, *The Cryosphere*, 7, 1411-1432, 2013.
16
17 Bolch, T., Sandberg, S. L., Simonsen, S.B., Mög, N., Machguth, H., P. Rastner, P., and Paul, F.: Mass loss
18 of Greenland's glaciers and ice caps 2003–2008 revealed from ICESat data, *Geophys. Res. Lett.*, 40, 875–
19 881, doi:10.1002/grl.50270, 2013.
20
21 Bonin, J. and Chambers, D.: Uncertainty estimates of a GRACE inversion modelling technique over
22 Greenland using a simulation, *Geophys J Int*, 194, 212-229, 2013.
23
24 Box, J., and Colgan, W.: Greenland Ice Sheet Mass Balance Reconstruction. Part III: Marine Ice Loss and
25 Total Mass Balance (1840–2010). *J. Climate*, 26, 6990–7002, doi: [http://dx.doi.org/10.1175/JCLI-D-12-](http://dx.doi.org/10.1175/JCLI-D-12-00546.1)
26 00546.1, 2013.
27
28 Chen, J., Wilson, C., Tapley, B., and Ries, J.: Low degree gravitational changes from GRACE: Validation
29 and interpretation, *Geophys Res Lett*, 31, 2004.
30
31 Cheng, M., Tapley, B. D., and Ries, J. C.: Deceleration in the Earth's oblateness, *J Geophys Res-Sol EA*,
32 118, 740-747, 2013.
33
34 Cogley, J. G.: Greenland accumulation: An error model, *J Geophys Res-Atmos* (1984–2012), 109, 2004.
35
36 Colgan, W., Box, J. E., Andersen, M. L., Fettweis, X., Csathó, B., Fausto, R. S., Van As, D., and Wahr, J.:
37 Greenland high-elevation mass balance: inference and implication of reference period (1961–90) imbalance,
38 *Ann. Glaciol*, 56, 105-117, DOI: <http://dx.doi.org/10.3189/2015AoG70A967>, 2015.
39
40 Colgan, W., Abdalati, W., Citterio, M., Csatho, B., Fettweis, X., Luthcke, S., Moholdt, G., and Stober, M.:
41 Hybrid inventory, gravimetry and altimetry (HIGA) mass balance product for Greenland and the Canadian
42 Arctic, *Remote Sens. Environ*, 168, 24–39, doi:10.1016/j.rse.2015.06.016, 2015.
43
44 Gardner, A. S., Moholdt, G., Cogley, J. G., Wouters, B., Arendt, A. A., Wahr, J., Berthier, E., Hock, R.,
45 Pfeffer, W. T., Kaser, G., Ligtenberg, S. R., Bolch, T., Sharp, M. J., Hagen, J. O., van den Broeke, M. R.,
46 and Paul, F.: A Reconciled Estimate of Glacier Contributions to Sea Level Rise: 2003 to 2009, *Science*, 340
47 (6134), 852-857, DOI:10.1126/science.1234532, 2013
48

- 1 Enderlin, E. M., Howat, I. M., Jeong, S., Noh, M. J., Angelen, J. H., and Broeke, M. R.: An improved mass
2 budget for the Greenland ice sheet, *Geophys Res Lett*, 41, 866-872, 2014.
3
- 4 Ettema, J., van den Broeke, M. R., van Meijgaard, E., van de Berg, W. J., Bamber, J. L., Box, J. E., and
5 Bales, R. C.: Higher surface mass balance of the Greenland ice sheet revealed by high-resolution climate
6 modeling, *Geophys Res Lett*, 36, L12501, doi:10.1029/2009GL038110, 2009.
7
- 8 Fettweis, X.: Reconstruction of the 1979–2006 Greenland ice sheet surface mass balance using the regional
9 climate model MAR, *The Cryosphere Discussions*, 1, 123-168, 2007.
10
- 11 Gallée, H. and Schayes, G.: Development of a three-dimensional meso- γ primitive equation model:
12 Katabatic winds simulation in the area of Terra Nova Bay, Antarctica, *Mon Weather Rev*, 122, 671-685,
13 1994.
14
- 15 Groh, A., Ewert, H., Fritsche, M., Rülke, A., Rosenau, R., Scheinert, M., and Dietrich, R.: Assessing the
16 Current Evolution of the Greenland Ice Sheet by Means of Satellite and Ground-Based Observations, *Surv*
17 *Geophys*, 1-22, 2014.
18
- 19 Hanna, E., Huybrechts, P., Janssens, I., Cappelen, J., Steffen, K., and Stephens, A.: Runoff and mass balance
20 of the Greenland ice sheet: 1958–2003, *J Geophys Res-Atmos* (1984–2012), 110, D13108,
21 doi:10.1029/2004JD005641, 2005.
22
- 23 Howat, I. M., Ahn, Y., Joughin, I., van den Broeke, M. R., Lenaerts, J., and Smith, B.: Mass balance of
24 Greenland's three largest outlet glaciers, 2000–2010, *Geophys. Res. Lett*, 38, L12501/1 - L12501/5,
25 doi:10.1029/2011GL047565, 2011.
26
- 27 Howat, I. M. and Eddy, A.: Multi-decadal retreat of Greenland's marine-terminating glaciers, *J Glaciol*, 57,
28 389-396, 2011.
29
- 30 Johannessen, O. M., Khvorostovsky, K., Miles, M. W., and Bobylev, L. P.: Recent ice-sheet growth in the
31 interior of Greenland, *Science*, 310, 1013-1016, 2005.
32
- 33 Jürgen, B., Kalyanmoy, D., Kaisa, M., and Roman S.: *Multiobjective Optimization: Interactive and*
34 *Evolutionary Approaches*, ISBN: 978-3-540-88907-6, 2008.
35
- 36 Kjeldsen, K. K., Khan, S. A., Wahr, J., Korsgaard, N. J., Kjær, K. H., Bjørk, A. A., Hurkmans, R., Broeke,
37 M. R., Bamber, J. L., and Angelen, J. H.: Improved ice loss estimate of the northwestern Greenland ice
38 sheet, *J Geophys Res-Sol EA*, 118, 698-708, 2013.
39
- 40 Luthcke, S. B., Sabaka, T., Loomis, B., Arendt, A., McCarthy, J., and Camp, J.: Antarctica, Greenland and
41 Gulf of Alaska land-ice evolution from an iterated GRACE global mascon solution, *J Glaciol*, 59, 613-631,
42 2013.
43
- 44 Luthcke, S. B., Zwally, H., Abdalati, W., Rowlands, D., Ray, R., Nerem, R., Lemoine, F., McCarthy, J., and
45 Chinn, D.: Recent Greenland ice mass loss by drainage system from satellite gravity observations, *Science*,
46 314, 1286-1289, 2006.
47
- 48 Moon, T., Joughin, I., Smith, B., Broeke, M. R., Berg, W. J., Nođ, B., and Usher, M.: Distinct patterns of
49 seasonal Greenland glacier velocity, *Geophys. Res. Lett*, 41, 7209-7216, 2014.
50

- 1 No ě, B., van de Berg, W. J., van Meijgaard, E., Kuipers Munneke, P., van de Wal, R. S. W., and van den
2 Broeke, M. R.: Evaluation of the updated regional climate model RACMO2.3: summer snowfall impact on
3 the Greenland Ice Sheet, *The Cryosphere*, 9, 1831-1844, doi:10.5194/tc-9-1831-2015, 2015.
4
- 5 Ohmura, A. and Reeh, N.: New precipitation and accumulation maps for Greenland, *J. Glaciol*, 37, 140-148,
6 1991.
7
- 8 Paulson, A., Zhong, S., and Wahr, J.: Inference of mantle viscosity from GRACE and relative sea level data,
9 *Geophys J Int*, 171, 497-508, 2007.
10
- 11 Peltier, W.: Global glacial isostasy and the surface of the ice-age Earth: the ICE-5G (VM2) model and
12 GRACE, *Annu. Rev. Earth Planet. Sci*, 32, 111-149, 2004.
13
- 14 Rignot, E., Box, J., Burgess, E., and Hanna, E.: Mass balance of the Greenland ice sheet from 1958 to 2007,
15 *Geophys Res Lett*, 35, L20502.1-L20502.5, doi:10.1029/2008GL035417, 2008.
16
- 17 Rignot, E. and Kanagaratnam, P.: Changes in the velocity structure of the Greenland Ice Sheet, *Science*,
18 311, 986-990, 2006.
19
- 20 Rignot, E., Velicogna, I., van den Broeke, M., Monaghan, A., and Lenaerts, J.: Acceleration of the
21 contribution of the Greenland and Antarctic ice sheets to sea level rise, *Geophys Res Lett*, 38, L05503.1-
22 L05503.5, doi:10.1029/2011GL046583, 2011.
23
- 24 Rodell, M., Houser, P., Jambor, U. e. a., Gottschalck, J., Mitchell, K., Meng, C., Arsenault, K., Cosgrove,
25 B., Radakovich, J., and Bosilovich, M.: The global land data assimilation system, *Bulletin of the American*
26 *Meteorological Society*, 85, 381-394, 2004.
27
- 28 Sasgen, I., Martinec, Z., and Bamber, J.: Combined GRACE and InSAR estimate of West Antarctic ice
29 mass loss, *J Geophys Res-Earth (2003–2012)*, 115, F04010, doi: 10.1029/2009JF001525, 2010.
30
- 31 Sasgen, I., van den Broeke, M., Bamber, J. L., Rignot, E., Sørensen, L. S., Wouters, B., Martinec, Z.,
32 Velicogna, I., and Simonsen, S. B.: Timing and origin of recent regional ice-mass loss in Greenland, *Earth*
33 *Planet SC Lett*, 333, 293-303, 2012.
34
- 35 Schrama, E. J. and Wouters, B.: Revisiting Greenland ice sheet mass loss observed by GRACE, *J Geophys*
36 *Res-Sol EA (1978–2012)*, 116, 377–385, doi: 10.1007/s10712-011-9113-7, 2011.
37
- 38 Schrama, E. J., Wouters, B., and Rietbroek, R.: A mascon approach to assess ice sheet and glacier mass
39 balances and their uncertainties from GRACE data, *J Geophys Res-Sol EA*, 2014.
40
- 41 Shepherd, A., Ivins, E. R., Geruo, A., Barletta, V. R., Bentley, M. J., Bettadpur, S., Briggs, K. H., Bromwich,
42 D. H., Forsberg, R., and Galin, N.: A reconciled estimate of ice-sheet mass balance, *Science*, 338, 1183-
43 1189, 2012.
44
- 45 Simpson, M. J., Milne, G. A., Huybrechts, P., and Long, A. J.: Calibrating a glaciological model of the
46 Greenland ice sheet from the Last Glacial Maximum to present-day using field observations of relative sea
47 level and ice extent, *Quaternary Sci Rev*, 28, 1631-1657, 2009.
48
- 49 Sørensen, L. S., Simonsen, S. B., Nielsen, K., Lucas-Picher, P., Spada, G., Adalgeirsdottir, G., Forsberg, R.,
50 and Hvidberg, C.: Mass balance of the Greenland ice sheet (2003-2008) from ICESat data-the impact of
51 interpolation, sampling and firn density, *The Cryosphere*, 5, 173-186, 2011.

- 1 Swenson, S., Wahr, J., and Milly, P.: Estimated accuracies of regional water storage variations inferred from
2 the Gravity Recovery and Climate Experiment (GRACE), *Water Resour Res*, 39, 11.1-11.3,
3 doi:10.1029/2002WR001808, 2003.
4
- 5 Swenson, S. and Wahr, J.: Post-processing removal of correlated errors in GRACE data, *Geophys Res Lett*,
6 33, L08402, doi:10.1029/2005GL025285, 2006.
7
- 8 Swenson, S., Chambers, D., and Wahr, J.: Estimating geocenter variations from a combination of GRACE
9 and ocean model output, *J Geophys Res-Sol EA (1978–2012)*, 113, 2008.
10
- 11 Tedesco, M., Fettweis, X., Mote, T., Wahr, J., Alexander, P., Box, J., and Wouters, B.: Evidence and
12 analysis of 2012 Greenland records from spaceborne observations, a regional climate model and reanalysis
13 data, *The Cryosphere*, 7, 2013.
14
- 15 Thomas, R., Csatho, B., Davis, C., Kim, C., Krabill, W., Manizade, S., McConnell, J., and Sonntag, J.: Mass
16 balance of higher-elevation parts of the Greenland ice sheet, *J Geophys Res-Atmos (1984–2012)*, 106,
17 33707-33716, 2001.
18
- 19 Tiwari, V. M., Wahr, J., and Swenson, S.: Dwindling groundwater resources in northern India, from satellite
20 gravity observations, *Geophys. Res. Lett.*, 36, L18401, doi:10.1029/2009GL039401, 2009.
21
- 22 Tikhonov, A. N.: Regularization of incorrectly posed problems, *Soviet Math. Dokl*, 1624-1627, 1963.
23
- 24 Uppala, S. M., Kållberg, P., Simmons, A., Andrae, U., Bechtold, V., Fiorino, M., Gibson, J., Haseler, J.,
25 Hernandez, A., and Kelly, G.: The ERA-40 re-analysis, *Q J Roy Meteor Soc*, 131, 2961-3012, 2005.
26
- 27 van Angelen, J., Lenaerts, J., Lhermitte, S., Fettweis, X., Kuipers Munneke, P., van den Broeke, M., and
28 Van Meijgaard, E.: Sensitivity of Greenland Ice Sheet surface mass balance to surface albedo
29 parameterization: a study with a regional climate model, *The Cryosphere*, 6, 2012.
30
- 31 van de Wal, R., Boot, W., Smeets, C., Snellen, H., van den Broeke, M., and Oerlemans, J.: Twenty-one
32 years of mass balance observations along the K-transect, West Greenland, *Earth system science data*
33 *discussions*, 5, 351-363, 2012.
34
- 35 van den Broeke, M., Bamber, J., Ettema, J., Rignot, E., Schrama, E., van de Berg, W. J., van Meijgaard, E.,
36 Velicogna, I., and Wouters, B.: Partitioning recent Greenland mass loss, *science*, 326, 984-986, 2009.
37
- 38 van der Wal, W., Barnhoorn, A., Stocchi, P., Gradmann, S., Wu, P., Drury, M., and Vermeersen, B.: Glacial
39 isostatic adjustment model with composite 3-D Earth rheology for Fennoscandia, *Geophys J Int*, 194, 61-
40 77, 2013.
41
- 42 Velicogna, I. and Wahr, J.: Time-variable gravity observations of ice sheet mass balance: Precision and
43 limitations of the GRACE satellite data, *Geophys Res Lett*, 40, 3055-3063, 2013.
44
- 45 Sutterley, T., and van den Broeke, M.: Regional acceleration in ice mass loss from Greenland and Antarctica
46 using GRACE time-variable gravity data, *Geophys Res Lett*, 8130–8137, doi: 10.1002/2014GL061052,
47 2014.
48
- 49 Vernon, C., Bamber, J., Box, J., van den Broeke, M., Fettweis, X., Hanna, E., and Huybrechts, P.: Surface
50 mass balance model intercomparison for the Greenland ice sheet, *The Cryosphere*, 7, 599-614, 2013.
51

- 1 Wahr, J., Molenaar, M., and Bryan, F.: Time variability of the Earth's gravity field: Hydrological and
2 oceanic effects and their possible detection using GRACE, *Journal of Geophysical Research*, 103, 30205-
3 30230,30229, 1998.
- 4 Wouters, B., Chambers, D., and Schrama, E.: GRACE observes small-scale mass loss in Greenland,
5 *Geophys Res Lett*, 35, L20501, doi:10.1029/2008GL034816, 2008.
- 6
- 7 Wouters, B., Bamber, J., van den Broeke, M., Lenaerts, J., and Sasgen, I.: Limits in detecting acceleration
8 of ice sheet mass loss due to climate variability, *Nat Geosci*, 6, 613-616, 2013.
- 9
- 10 Xu, Z., Schrama, E., and van der Wal, W.: Optimization of regional constraints for estimating the Greenland
11 mass balance with GRACE level-2 data, *Geophys J Int*, 202, 381-393, 2015.
- 12
- 13 Zwally, H. and Giovinetto, M.: Spatial distribution of net surface mass balance on Greenland, *Ann Glaciol*,
14 31, 126-132, 2000.
- 15
- 16 Zwally, H., Schutz, B., Abdalati, W., Abshire, J., Bentley, C., Brenner, A., Bufton, J., Dezio, J., Hancock,
17 D., and Harding, D.: ICESat's laser measurements of polar ice, atmosphere, ocean, and land, *J Geodyn*, 34,
18 405-445, 2002.
- 19
- 20 Zwally, H. J., Giovinetto, M. B., Li, J., Cornejo, H. G., Beckley, M. A., Brenner, A. C., Saba, J. L., and Yi,
21 D.: Mass changes of the Greenland and Antarctic ice sheets and shelves and contributions to sea-level rise:
22 1992–2002, *J Glaciol*, 51, 509-527, 2005.
- 23
- 24 Zwally, H. J., Jun, L., Brenner, A. C., Beckley, M., Cornejo, H. G., Dimarzio, J., Giovinetto, M. B.,
25 Neumann, T. A., Robbins, J., and Saba, J. L.: Greenland ice sheet mass balance: distribution of increased
26 mass loss with climate warming; 200307 versus 19922002, *J Glaciol*, 57, 88-102, 2011.
- 27
- 28 Zwally, H. J., Mario B. Giovinetto, Matthew A. Beckley, and Jack L. Saba:
29 http://icesat4.gsfc.nasa.gov/cryo_data/ant_grn_drainage_systems.php, last access: 09-02-2015, 2012.